

# Simulator-free Solution of High-dimensional Stochastic Elliptic Partial Differential Equations using Deep Neural Networks

Sharmila Karumuri, Rohit Tripathy, Ilias Bilionis\*, Jitesh Panchal

*School of Mechanical Engineering,  
585 Purdue Mall, Purdue University, West Lafayette, IN 47907-2088, USA*

---

## Abstract

Stochastic partial differential equations (SPDEs) are ubiquitous in engineering and computational sciences. The stochasticity arises as a consequence of uncertainty in input parameters, constitutive relations, initial/boundary conditions, etc. Because of these functional uncertainties, the stochastic parameter space is often high-dimensional, requiring hundreds, or even thousands, of parameters to describe it. This poses an insurmountable challenge to response surface modeling since the number of forward model evaluations needed to construct an accurate surrogate grows exponentially with the dimension of the uncertain parameter space; a phenomenon referred to as the *curse of dimensionality*. State-of-the-art methods for high-dimensional uncertainty propagation seek to alleviate the curse of dimensionality by performing dimensionality reduction in the uncertain parameter space. However, one still needs to perform forward model evaluations that potentially carry a very high computational burden. We propose a novel methodology for high-dimensional uncertainty propagation of elliptic SPDEs which lifts the requirement for a deterministic forward solver. Our approach is as follows. We parameterize the solution of the elliptic SPDE using a deep residual network (ResNet). In a departure from traditional mean

---

\*Corresponding author

*Email addresses:* [skarumur@purdue.edu](mailto:skarumur@purdue.edu) (Sharmila Karumuri), [rtripath@purdue.edu](mailto:rtripath@purdue.edu) (Rohit Tripathy), [ibilion@purdue.edu](mailto:ibilion@purdue.edu) (Ilias Bilionis), [panchal@purdue.edu](mailto:panchal@purdue.edu) (Jitesh Panchal)  
*URL:* <https://www.predictivesciencelab.org/> (Ilias Bilionis)

squared error (MSE) loss function for training the ResNet, we introduce a novel physics-informed loss function derived from variational principles. Specifically, our loss function is the expectation of the energy functional of the PDE over the stochastic variables. We demonstrate our solver-free approach on the steady state heat equation with high dimensional random thermal conductivity in the order of 100 and 200 for one dimensional and two-dimensional problem respectively.

*Keywords:* stochastic elliptic partial differential equations, deep neural networks, residual networks, energy functional, stochastic heat equation, physics-informed

---

## 1. Introduction

With the rapid increase in computing resources [1], numerical methods for the solution of partial differential equations (PDEs) that govern physical systems have become an integral part of modern computational science [2]. In many engineering/scientific applications of interest, inputs to the governing PDEs are unknown exactly. Such uncertainties are modeled using the framework of probability theory, thereby giving rise to *stochastic partial differential equations* (SPDEs). The uncertainty in input data can arise from multiple sources - unknown (or partially known) material properties / constitutive relationships, external loads, initial conditions (ICs), boundary conditions (BCs), physical geometry (arising from manufacturing imperfections), etc. Naturally, this leads to the question of how to ensure reliable and robust predictions of the behavior of the physical system under consideration. Answering this question is at the heart of research efforts in the field of uncertainty quantification (UQ) [3, 4]. In particular, the probabilistic assessment of the effect of input uncertainties on output quantities of interest (QoI) is known as the forward UQ or uncertainty propagation (UP) problem.

The most straightforward approach to tackling the UP problem is the Monte Carlo (MC) method [5]. The MC approach can be summarized as follows - one can obtain estimates of the statistics of QoIs by computing averages over random samples. The variance of the MC estimate vanishes in the limit of infinite samples. A remarkable feature of the MC method is that the statistical convergence of the MC estimate is independent of the number of the stochastic dimensions. This makes MC method a highly attractive tool for numerical integration, especially in high dimensions. Consequently, the MC method and its advanced variants have been extensively applied to a variety of UQ problems [6, 7, 8, 9, 10]. Unfortunately, the number of samples needed to obtain convergent statistics from the MC method is typically large. This makes the application of MC unfeasible for UP in sophisticated modern PDE solvers because of the high computational cost associated with generating each individual

sample of the QoI.

The standard approach to dealing with expensive numerical PDE solvers is to replace them with a cheap-to-evaluate surrogate model (or response surface). The idea of the surrogate approach is that one can utilize information collected from a finite number of runs of the expensive PDE solver on carefully selected (and potentially adaptive) input locations, to construct a map that links the input uncertain parameters to the QoIs. Since the surrogate is cheap to evaluate, one can apply standard MC methods to propagate uncertainties through the PDE. This approach to tackling the UP problem has been applied with great success on a very diverse set of applications with moderate stochastic dimensionality, such as fracture mechanics [11], biological systems [12], molecular dynamics [13], nuclear engineering [14], etc. Traditional choices for surrogate models include Gaussian process regression (GPR) (or Kriging) [15, 16, 17, 18, 19], polynomial chaos expansion [20, 21, 22, 23], and radial basis functions [24, 25].

Inspite of the indisputable success of traditional surrogate models on tasks with low/moderate stochastic dimensionality, approaches such as Gaussian processes and polynomial chaos have not been successfully scaled to high dimensions. The task of constructing a response surface becomes exponentially difficult as the number of input dimensions increases, a phenomenon widely referred to as the *curse of dimensionality* [26]. The implication of the curse of dimensionality is, essentially, that as the input dimensionality grows linearly, one has to perform an exponentially increasing number of forward model evaluations to maintain the accuracy of the response surface. In fact, if one considers the task of approximating a generic nonlinear, multivariate function with scalar response, the computational time needed for performing sufficient forward model evaluations quickly becomes unfeasible even for inexpensive computer codes [27].

Given that the naive construction of response surfaces with high stochastic dimensionality is a futile approach, a typical workaround is to perform *dimensionality reduction* on the stochastic parameter space. The simplest approach to dimensionality reduction involves a ranking of the input dimensions in or-

der of importance and then rejecting ‘unimportant’ dimensions. This is the approach adopted by methods such as sensitivity analysis [28] and automatic relevance determination [29]. The most common approach to dimensionality reduction involves projecting stochastic inputs onto a low-dimensional manifold. In applications characterized by functional uncertainties (such as flow through porous media), the infinite dimensional uncertainty is reduced to finite dimensions through the celebrated Karhunen-Loéve expansion (KLE) [30]. The KLE involves computing the eigendecomposition of the covariance function of the uncertain parameter and using the decay of the eigenvalues to approximate the infinite dimensional uncertainty as a linear combination of the orthogonal eigenfunctions (corresponding to the retained eigenvalues). In essence this procedure is a linear projection of the input uncertainty onto a finite dimensional vector subspace. Analogously, when the uncertain parameters are finite dimensional, a linear projection is performed on the basis of the eigendecomposition of an empirical covariance matrix. In the machine learning (ML) community, this is commonly referred to as the *principal component analysis* (PCA) [31]. Although KLE and PCA have been applied successfully to numerous applications, they overestimate the intrinsic dimensionality because of the fact they (i) recover *only* linear manifolds in the input space, and (ii) do not take into consideration information in the model outputs. Kernel principal component analysis (KPCA) [32, 33] alleviates the first drawback of the aforementioned techniques by performing the eigendecomposition on a high (potentially infinite) dimensional space obtained through a nonlinear transformation of the original inputs. The recently popularized method of active subspaces (AS) [34, 35, 36, 37, 38, 39, 40], on the other hand, performs linear dimensionality reduction by performing eigendecomposition on an empirical covariance matrix constructed from samples of the model output gradients - thereby alleviating the second drawback. To bypass the necessity of obtaining gradients (often unfeasible for sophisticated PDE solvers), [19] proposed a methodology wherein the orthogonal AS transformation is subsumed into the covariance kernel of GPR. Finally, recent work from [41] overcomes both limitations, by using DNNs to

generalize the gradient-free approach to AS by recovering nonlinear manifolds in the input space. At the same time, [42] recast the surrogate modeling task as an image-to-image regression problem, mapping a snapshot of the input uncertainty to a snapshot of the PDE solution. By leveraging recent advances in deep convolutional networks, the authors demonstrate this approach on challenging high-dimensional surrogate modeling tasks in heterogeneous media [42, 43].

While rapid strides have been made in the developing techniques for high dimensional surrogate models, a fundamental limitation of existing methodologies is that one must still perform repeated evaluations of the forward PDE solver. Dimensionality reduction in the stochastic parameter space and adaptive design of experiments can only take one so far. In this work, we approach the task of UP through SPDEs with high dimensional uncertainties with a novel paradigm freed from the shackles of deterministic PDE solvers. The summary of our approach is that we seek to approximate the field variables in SPDEs as a parameterized function of all relevant input parameters. These include the stochastic parameters, spatial/temporal, etc. We seek a flexible parameterization of the field variables which can accurately approximate complex nonlinear maps and has closed-form gradients with respect to the input variables. Naturally, the function approximator of choice to represent the solution of SPDE is DNNs; specifically we use a deep residual network [44, 45, 46]. DNNs are a class of highly flexible and scalable nonlinear function approximators [47]. It is well-known that under mild conditions, neural networks with a single hidden layer are universal function approximators [48]. While the idea of DNNs is not novel, their usage in practical applications is rather recent - thanks in large part to the widespread availability of cheap computing resources, the active development and maintainence of powerful automatic differentiation (AD) capable libraries such as `Tensorflow` [49], `PyTorch` [50], `MxNet` [51], and theoretical advances in stochastic optimization [52, 53, 54]. Furthermore, in a departure from mean squared PDE residual minimization used in related works [55, 56], we leverage the variational principle associated with the analogous deterministic PDE and formulate an energy functional for the SPDE by computing an expectation over

the stochastic parameters. The SPDE is then solved by minimizing the energy functional with respect to the DNN parameters.

Our work is closely related to the ‘Deep Ritz method’ for the solution of deterministic PDEs from variational principles [57] using DNNs. In particular, we focus our attention on the elliptic SPDE; although the described methodology is more generally applicable. This paper is also closely related to recent work from [58] in which the authors proposed a methodology to construct Bayesian deep convolutional network surrogate models for SPDEs without access to a deterministic PDE solver by leveraging the variational formulation of the PDE.

This manuscript is organized as follows. We begin with a discussion of the variational formulation of the stochastic elliptic PDE problem in Sec. 2.1 and prove that the solution of the corresponding stochastic boundary value problem (SBVP) minimizes an energy functional. In Sec. 2.2, we discuss about characterizing the random fields with finite number of variables. We propose a construction for the trial solution in Sec. 2.3 which automatically satisfies the essential (i.e., Dirichlet) boundary conditions and move onto a discussion of deep residual networks (ResNet) in Sec. 2.4 - our function approximator of choice for this work. In Sec. 2.5, we discuss the formulation of the ResNet training as a stochastic minimization of the proposed energy functional loss. In Sec. 3, we demonstrate our methodology on 1D and 2D elliptic SPDE problems with high dimensional input uncertainty in the conductivity coefficient. Finally, Sec. 4 is devoted to the concluding remarks and an outlook on future work.

## 2. Methodology

### 2.1. Variational formulation of stochastic elliptic partial differential equations

Let  $(\Omega, \mathcal{F}, \mathbb{P})$  be a probability space, where  $\Omega$  is the sample space,  $\mathcal{F}$  a  $\sigma$ -algebra of events, and  $\mathbb{P}$  a probability measure. We follow the standard notation where upper case letters denote random quantities and lower case letters their values. Let  $\mathcal{X} \subset \mathbb{R}^d$  be the spatial domain of interest with dimension  $d = 1, 2$ , or 3. We assume that  $\mathcal{X}$  has a Lipschitz boundary consisting of two disjoint parts  $\Gamma_D$  and  $\Gamma_N$ . We will denote points in  $\mathcal{X}$  by  $x$ .

We are interested in approximating the stochastic process (s.p.)  $U : \mathcal{X} \times \Omega \rightarrow \mathbb{R}$  which solves the stochastic elliptic PDE (SEPDE):

$$-\nabla \cdot (A(x, \omega) \nabla U(x, \omega)) + C(x, \omega) U(x, \omega) = F(x, \omega), \text{ in } x \in \mathcal{X}, \quad (1)$$

almost surely (a.s) with Dirichlet and Neumann boundary conditions given by

$$U(x, \omega) = G_D(x, \omega) \text{ on } x \in \Gamma_D, \quad (2)$$

a.s. and

$$n^T(x) (A(x, \omega) \nabla U(x, \omega)) = G_N(x, \omega), \text{ on } x \in \Gamma_N \quad (3)$$

a.s., respectively, where  $n(x)$  is the normal to the boundary  $\Gamma_N$  at  $x$  on  $\Gamma_N$ , where  $C, F, G_D, G_N$  are scalar s.p.'s, and  $A$  is symmetric  $d \times d$  matrix s.p.

We derive a variational principle for the above stochastic boundary value problem (SBVP) in the form of the following theorem which constitutes the main result of the paper.

**Theorem 1.** *Variational formulation of SEPDEs. Let  $C \in L^\infty(\mathcal{X} \times \Omega)$ ,  $F \in L^2(\mathcal{X} \times \Omega)$ ,  $G_D \in L^2(\Gamma_D \times \Omega)$ ,  $G_N \in L^2(\Gamma_N \times \Omega)$ . Assume that  $A \in L^2(\mathcal{X} \times \Omega, \mathbb{R}^{d \times d})$  and that it is a.s. uniformly elliptic, i.e., there exists an  $\alpha > 0$  such that*

$$\sum_{i,j=1}^d A_{ij}(x, \omega) v_i v_j \geq \alpha \|v\|^2, \text{ for all } v \in \mathbb{R}^d \text{ and } x \in \mathcal{X} \text{ a.s.}, \quad (4)$$

and that  $C \geq \eta > 0$  a.s. Then the SBVP defined by Eqs. (1), (2), and (3) has a unique solution  $U^*$  in:

$$\mathcal{U} := \left\{ U : \mathcal{X} \times \Omega \rightarrow \mathbb{R} \text{ s.t. } \mathbb{E} \left[ \int_{\mathcal{X}} (\| \nabla U \|^2 + U^2) dx \right] < \infty, \right. \\ \left. \text{and } U|_{\Gamma_D} = G_D \text{ a.s.} \right\}, \quad (5)$$

and this solution minimizes the functional:

$$J[U] := \mathbb{E} \left[ \int_{\mathcal{X}} \left\{ \frac{1}{2} (A \nabla U \cdot \nabla U + C U^2) - F U \right\} dx - \int_{\Gamma_N} G_N U d\Gamma_N \right]. \quad (6)$$

Here  $\mathbb{E}$  is an expectation over stochastic parameter  $\omega$ .

*Proof.* The proof consists of three parts. We start by proving that the problem of minimizing  $J[U]$  has a unique solution  $U^*$  in  $\mathcal{U}$ . Then, we show that for almost all  $\omega$ ,  $U^*(\cdot, \omega)$  satisfies the weak form of the BVP. Finally, we show that any solution of the weak form of the BVP is a stationary point of  $J[U]$ .

*Part 1: Existence and uniqueness of variational minimum.* Consider the following Hilbert space

$$\mathcal{H} := \left\{ U : \mathcal{X} \times \Omega \rightarrow \mathbb{R} \text{ s.t. } \mathbb{E} \left[ \int_{\mathcal{X}} (\| \nabla U \|^2 + U^2) dx \right] < \infty \right\}, \quad (7)$$

with inner product

$$\langle U, V \rangle_{\mathcal{H}} := \mathbb{E} \left[ \int_{\mathcal{X}} (\nabla U \cdot \nabla V + U V) dx \right], \quad (8)$$

and the corresponding norm

$$\| U \|_{\mathcal{H}} := \langle U, U \rangle_{\mathcal{H}}^{\frac{1}{2}}. \quad (9)$$

Notice that

$$J[U] = \frac{1}{2} B[U, U] - T[U],$$

where

$$B[U, V] := \mathbb{E} \left[ \int_{\mathcal{X}} (A \nabla U \cdot \nabla V + C U V) dx \right] \quad (10)$$

is a bounded bilinear form and

$$T[U] = \mathbb{E} \left[ \int_{\mathcal{X}} F U dx + \int_{\Gamma_N} G_N U d\Gamma_N \right] \quad (11)$$

is a bounded linear functional. Finally, define the test space

$$\mathcal{V} := \left\{ V : \mathcal{X} \times \Omega \rightarrow \mathbb{R} \text{ s.t. } \mathbb{E} \left[ \int_{\mathcal{X}} (\| \nabla V \|^2 + V^2) dx \right] < \infty, \right. \\ \left. \text{and } V|_{\Gamma_D} = 0 \text{ a.s.} \right\}, \quad (12)$$

a subspace of  $\mathcal{H}$ . Notice that  $\mathcal{U}$  is an affine subspace of  $\mathcal{H}$ , i.e.,  $\mathcal{U} = \tilde{G}_D + \mathcal{V}$  where  $\tilde{G}_D$  is a suitable extension of  $G_D$  to the entire  $\mathcal{X} \times \Omega$ .

The first variation of  $J[U]$  with respect to a  $V$  in  $\mathcal{V}$  is

$$\begin{aligned} \frac{\delta J[U]}{\delta V} &:= \lim_{\epsilon \rightarrow 0} \frac{J[U + \epsilon V] - J[U]}{\epsilon} \\ &= \lim_{\epsilon \rightarrow 0} \frac{\frac{1}{2} B[U + \epsilon V, U + \epsilon V] - T[U + \epsilon V] - \frac{1}{2} B[U, U] + T[U]}{\epsilon} \\ &= \lim_{\epsilon \rightarrow 0} \frac{\frac{1}{2} B[U, U] + \epsilon B[V, U] + \frac{1}{2} \epsilon^2 B[V, V] - T[U] - \epsilon T[V] - \frac{1}{2} B[U, U] + T[U]}{\epsilon} \\ &= B[V, U] - T[V]. \end{aligned} \quad (13)$$

Since any local minimum of  $J[U]$  must have a vanishing first variation, it suffices to show that the problem of finding a  $U \in \mathcal{U}$  such that

$$B[V, U] = T[V], \quad (14)$$

for all  $V \in \mathcal{V}$ , has a unique solution. This is guaranteed by the Lax-Milgram theorem if we show that  $B$  is coercive. Indeed, we have:

$$\begin{aligned} B[V, V] &= \mathbb{E} \left[ \int_{\mathcal{X}} (A \nabla V \cdot \nabla V + C V^2) dx \right] \\ &\geq \mathbb{E} \left[ \int_{\mathcal{X}} (\alpha \| \nabla V \|^2 + \eta V^2) dx \right] \\ &\geq \min\{\alpha, \eta\} \| V \|_{\mathcal{H}}^2. \end{aligned} \quad (15)$$

This concludes the proof that  $J[U]$  has a unique minimum  $U^* \in \mathcal{U}$ .

*Part 2: The extremum  $U^*$  solves a.s. the weak form of the BVP.* Pick  $V(x, \omega) = v(x)\Phi(\omega)$  for a  $v$  in the Sobolev space  $H_0^1(\mathcal{X}, \Gamma_D)$  and  $\Phi \in L^2(\Omega)$ . Eq. (14)

implies that:

$$\begin{aligned}
B[v\Phi, U^*] &= T[v\Phi] \\
\Rightarrow \mathbb{E} \left[ \int_{\mathcal{X}} (A \nabla U^* \cdot \nabla(v\Phi) + CU^*(v\Phi)) dx \right] &= \mathbb{E} \left[ \int_{\mathcal{X}} F(v\Phi) dx + \int_{\Gamma_N} G_N(v\Phi) d\Gamma_N \right] \\
\Rightarrow \mathbb{E} \left[ \Phi \int_{\mathcal{X}} (A \nabla U^* \cdot \nabla v + CU^*) dx \right] &= \mathbb{E} \left[ \Phi \left\{ \int_{\mathcal{X}} F v dx + \int_{\Gamma_N} G_N v d\Gamma_N \right\} \right],
\end{aligned}$$

and since  $\Phi(\omega)$  is arbitrary:

$$\int_{\mathcal{X}} (A \nabla U^* \cdot \nabla v + CU^* v) dx = \int_{\mathcal{X}} F v dx + \int_{\Gamma_N} G_N v d\Gamma_N \text{ a.s.}, \quad (16)$$

i.e.,  $U^*(\cdot, \omega)$  satisfies the weak formulation of the BVP a.s.

*Part 3: Any weak solution of the BVP solves the variational problem.* This is readily seen by following the arguments of Part 2 backwards.  $\square$

**Remark 1.** Note that it is also possible to prove the theorem for  $C = 0$ . To prove this, notice that:

$$\begin{aligned}
B[V, V] &= \mathbb{E} \left[ \int_{\mathcal{X}} (A \nabla V \cdot \nabla V) dx \right] \\
&\geq \mathbb{E} \left[ \int_{\mathcal{X}} (\alpha \|\nabla V\|^2) dx \right] \\
&= \alpha \mathbb{E} \left[ \int_{\mathcal{X}} \|\nabla V\|^2 dx \right] \\
&\geq \alpha \rho \mathbb{E} \left[ \int_{\mathcal{X}} (\|\nabla V\|^2 + V^2) dx \right] \\
&= \alpha \rho \|V\|_{\mathcal{H}}^2,
\end{aligned} \quad (17)$$

for some  $\rho > 0$  that depends only on the Lebesgue measure of  $\mathcal{X}$  and on its dimension. Here, going from the third to the fourth step we used the fact that the  $H^1$  seminorm and the  $H^1$  norm are equivalent in  $H_0^1(\mathcal{X})$ , see Chapter 1 of [59].

## 2.2. Characterization of the random fields using a finite number of variables

From this point on, we assume that the random fields  $A, C, F, G_D, G_N$  can be approximated with the random vector  $\Xi$  in  $\mathbb{R}^{d_\xi}$ . For example, this approximation could be the result of employing the Karhunen-Loëve theorem [30, 60], a non-linear dimensionality reduction technique on empirical data [61, 33], or even

raw high-dimensional data such as pictures [42, 58]. That is, we substitute in  $J$ ,  $A(x, \omega) \approx a(x, \Xi(\omega))$ ,  $C(x, \omega) \approx c(x, \Xi(\omega))$ ,  $F(x, \omega) \approx f(x, \Xi(\omega))$ ,  $G_D(x, \omega) \approx g_d(x, \Xi(\omega))$ ,  $G_N(x, \omega) \approx g_n(x, \Xi(\omega))$  and we restrict the space  $\mathcal{U}$  accordingly. We denote the solution of this “simpler” SBVP as a function  $u^*(x, \Xi(\omega))$ .

The simplification of the random fields induces an error in the solution of the SBVP, i.e., the processes  $U^*(x, \omega)$  and  $u^*(x, \Xi(\omega))$  differ. However, this error depends on the specific technique one uses to simplify the random fields and one can find several case studies in the literature [60]. Since in this paper we develop a methodology that is agnostic to the details of the random field, we refrain from studying this approximation error.

### 2.3. Extension to boundary conditions:

The solution of the “simpler” SBVP  $u^*(x, \Xi(\omega))$  is obtained by minimizing the functional in Eq. (6). Note that Neumann boundary conditions  $G_N$  are already included in the functional  $J$ , but the Dirichlet boundary conditions  $G_D$  (see Eq. (5)) have to be imposed as constraints leading to a constrained optimization problem.

The resulting constrained optimization problem may be addressed in a number of ways. One way to impose the Dirichlet condition on Eq. (6) is by using constrained optimization methods such as penalty formulations [55, 57], Lagrange multipliers, or active set methods [62]. Another way is to model  $u(x, \Xi(\omega))$  in such a way that the constraints are automatically satisfied by construction, thus changing the original constrained optimization problem to an unconstrained one [63]. We resort to the latter way by writing  $u(x, \Xi(\omega))$  as the sum of two terms [63],

$$u(x, \Xi(\omega)) = B(x, \Xi(\omega)) + K(x)N(x, \Xi(\omega)), \quad (18)$$

where  $N(x, \Xi(\omega))$  is approximated using a deep residual network (see Sec. 2.4) with inputs as  $x$  and  $\Xi(\omega)$ . The term  $B(x, \Xi(\omega))$  contains no adjustable parameters and ensures that the Dirichlet boundary conditions are satisfied. The second term  $K(x)$  is constructed such that it becomes zero on the Dirichlet

boundary.  $B$  and  $K$  can also be formulated as DNNs given boundary data [64]. In this work, we limit ourselves to a manual construction of  $B$  and  $K$  without using DNNs.

#### 2.4. The space of deep residual neural networks

We represent  $N(x, \Xi(\omega))$  with a DNN. In particular,  $N(x, \Xi(\omega))$  is chosen to be a deep residual network or ‘ResNet’ [44]. It has been empirically demonstrated in numerous works that adding residual blocks is an effective method for combating the problem of vanishing gradients and consequently allow robust training of deeper networks [65, 66, 67]. Furthermore, deep ResNets have, recently, been successfully applied to the task of data driven approximation of governing equations of dynamical systems in [46].

We denote the approximation of  $N(x, \Xi(\omega))$  as  $\widehat{N}(x, \Xi(\omega); \theta)$  where ‘ $\theta$ ’ are parameters (i.e. weights and biases) of the ResNet. The network accepts as input,  $x$  and  $\Xi(\omega)$ , and produces the output  $\widehat{N}(x, \Xi(\omega); \theta)$ , i.e., it defines a map from  $\mathbb{R}^m$ ,  $m = d + d_\xi$ , to  $\mathbb{R}$ .

The structure of the deep ResNet is as follows. We begin with a ‘dense layer’(or fully connected layer) which performs a linear transformation of the  $m$ -dimensional input into a  $n$ -dimensional space. The output of the computation from this initial dense layer is passed through  $K$  ‘residual’ blocks, each with  $L$  dense layers having ‘ $n$ ’ neurons each and with activation function imposed. Finally the output from this computation is passed through a dense layer which performs linear transformation of the  $n$ -dimensional output to a single value  $\widehat{N}(x, \Xi(\omega); \theta)$ .

The residual blocks differentiate classic DNNs from ResNets. A residual block comprises of an additional residual connection between its input and output, i.e., the original input to a residual block is added to the block activation before passing on to the next stage of computation in the network. A schematic of a residual block is shown in the Fig. 1a. Of the numerous choices for the nonlinear activation function in our deep networks, we elect to use the so-called

‘Swish’ activation function, which is defined as follows:

$$\sigma(z) = zS(\beta z) = \frac{z}{1 + e^{-(\beta z)}}, \quad (19)$$

where,  $S$  is the sigmoid activation function and  $\beta$  is either a user-defined or a tunable parameter. The Swish function was introduced in [68], who empirically demonstrated the superiority of this activation function compared to standard rectified linear unit or ReLU activation function, for training very deep networks. In this work,  $\beta$  is set to 1.

Mathematically, we start with the inputs  $x$  and  $\Xi(\omega)$  and we have:

$$z^{(1,0)} = W_0^{(1,0)}x + W_1^{(1,0)}\Xi(\omega) + b^{(1,0)}, \quad (20)$$

followed by

$$z^{(i,1)} := \sigma \left( W^{(i,1)}z^{(i-1,0)} + b^{(i,1)} \right), \quad (21)$$

$$z^{(i,j)} := \sigma \left( W^{(i,j)}z^{(i,j-1)} + b^{(i,j)} \right), \quad (22)$$

$$z^{(i,0)} := z^{(i,L)} + z^{(i-1,0)}, \quad (23)$$

for blocks  $i = 2, \dots, (K + 1)$  and for layers  $j = 2, \dots, L$ . Finally, we end with

$$\widehat{N}(x, \Xi(\omega); \theta) = z^{(K+2)} := \left( z^{(K+1,0)} \right)^T w^{(K+2)} + b^{(K+2)}. \quad (24)$$

The quantities  $W_0^{(1,0)} \in \mathbb{R}^{n \times d}$ ,  $W_1^{(1,0)} \in \mathbb{R}^{n \times d_\xi}$ ,  $W^{(i,j)} \in \mathbb{R}^{n \times n}$ ,  $w^{(K+2)} \in \mathbb{R}^n$  and  $b^{(i,j)} \in \mathbb{R}^n$ ,  $b^{(K+2)} \in \mathbb{R}$  are the weights and bias parameters, respectively.

Collectively, we denote all these parameters by  $\theta$ .

The last term in Eq. (23) which is the the residual connection helps to ease the training of the network [44]. The schematic of our deep ResNet with an initial dense layer followed by  $K$  residual blocks and an output linear layer is shown in the Fig. 1b.

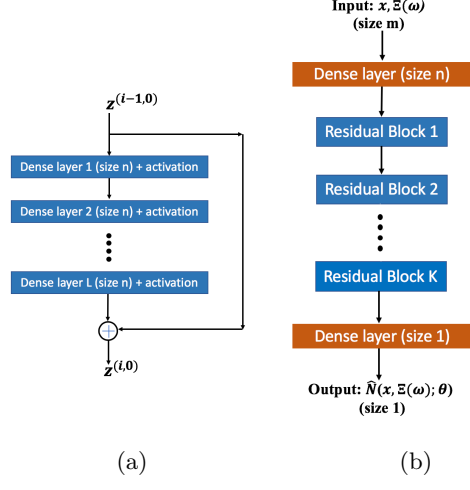


Figure 1: 1a shows a single residual block and 1b shows schematic of our deep ResNet

### 2.5. Training the ResNet

We plug the approximation  $\hat{N}(x, \Xi(\omega); \theta)$  into Eq. (18) leading to the following expression for the solution of the SBVP:

$$\hat{u}(x, \Xi(\omega); \theta) = B(x, \Xi(\omega)) + K(x) \hat{N}(x, \Xi(\omega); \theta). \quad (25)$$

Consequently, the energy functional,  $J$ , is now a function of the free parameters  $\theta$ :

$$J(\theta) := J[\hat{u}(x, \Xi(\omega); \theta)]. \quad (26)$$

Therefore, the task of training the ResNet is equivalent to solving the following unconstrained optimization task:

$$\theta^* = \arg \min_{\theta} J(\theta), \quad (27)$$

Note that the variational problem obtained in the end i.e.  $J(\theta)$  is not convex despite the fact that the initial problem  $J[U]$  is convex.

To proceed, consider the sampling average approximation:

$$\begin{aligned}
\hat{J}(\theta) := & \frac{|X|}{N_\xi} \sum_{k=1}^{N_\xi} \left\{ \frac{1}{N_x} \sum_{i=1}^{N_x} \left[ \frac{1}{2} \left[ a(X^{(ki)}, \Xi^{(k)}) \nabla_x \hat{u}(X^{(ki)}, \Xi^{(k)}; \theta) \cdot \nabla_x \hat{u}(X^{(ki)}, \Xi^{(k)}; \theta) \right. \right. \right. \\
& \left. \left. \left. + c(X^{(ki)}, \Xi^{(k)}) \hat{u}^2(X^{(ki)}, \Xi^{(k)}; \theta) \right] - f(X^{(ki)}, \Xi^{(k)}) \hat{u}(X^{(ki)}, \Xi^{(k)}; \theta) \right] \right\} \\
& - \frac{|X_b|}{N_\xi} \sum_{k=1}^{N_\xi} \left\{ \frac{1}{N_b} \sum_{r=1}^{N_b} \left[ g_n(X_b^{(kr)}, \Xi^{(k)}) \hat{u}(X_b^{(kr)}, \Xi^{(k)}; \theta) \right] \right\}, \tag{28}
\end{aligned}$$

where  $\Xi^{(k)}, k = 1, \dots, N_\xi$  are independent identically distributed (iid) replicas of  $\Xi$ ,  $X^{(ki)}, i = 1, \dots, N_x, k = 1, \dots, N_\xi$  are iid r.v.'s uniformly distributed in  $\mathcal{X}$ ,  $X_b^{(kr)}, r = 1, \dots, N_b, k = 1, \dots, N_\xi$  are iid r.v.'s uniformly distributed on the Neumann boundary  $\Gamma_n$ ,  $|X|$  is the Lebesgue measure of the spatial domain  $\mathcal{X}$  and  $|X_b|$  is the Lebesgue measure of the Neumann boundary  $\Gamma_n$ . It is trivial to see that  $\hat{J}$  is an unbiased Monte Carlo estimate of the energy functional  $J$ . Thus, the ResNet training is recast into a stochastic minimization problem:

$$\theta^* = \arg \min_{\theta} \mathbb{E}[\hat{J}(\theta)]. \tag{29}$$

The unconstrained optimization problem in Eq. (29) is solved through the adaptive moments (ADAM) optimization method [52], a robust variant of stochastic gradient descent (SGD) [69]. The ADAM's update scheme is given by:

$$\begin{aligned}
\mathbf{m}_{j+1} & \leftarrow \beta_1 \mathbf{m}_j + (1 - \beta_1) \nabla_{\theta} \hat{J}(\theta_j), \\
\mathbf{v}_{j+1} & \leftarrow \beta_2 \mathbf{v}_j + (1 - \beta_2) [\nabla_{\theta} \hat{J}(\theta_j)]^2, \\
\widetilde{\mathbf{m}}_{j+1} & \leftarrow \frac{\mathbf{m}_{j+1}}{1 - \beta_1}, \\
\widetilde{\mathbf{v}}_{j+1} & \leftarrow \frac{\mathbf{v}_{j+1}}{1 - \beta_2}, \\
\theta_{j+1} & \leftarrow \theta_j - \alpha \frac{\widetilde{\mathbf{m}}_{j+1}}{\sqrt{\widetilde{\mathbf{v}}_{j+1}} + \epsilon}, \tag{30}
\end{aligned}$$

where  $\alpha$  is a positive learning rate,  $\epsilon$  is a small positive number used to prevent zero in the denominator,  $\beta_1$  and  $\beta_2$  are averaging parameters which are, in principle, tunable. In practice, default values of  $\beta_1 = 0.9$ ,  $\beta_2 = 0.999$ , as suggested by [52] work well and we do not change these quantities.

In the loss function  $\hat{J}(\theta)$  of Eq. (28) we obtain the required derivatives using automatic differentiation (AD) [45] in `TensorFlow` [70]. The exact gradient of the loss function needed for the ADAM update in Eq. (30) is obtained using backpropagation [71].

### 3. Numerical examples

#### 3.1. Stochastic boundary value problem in 1D

Consider the following elliptic SBVP which models the steady-state heat conduction on a unit length domain:

$$-\nabla \cdot (A(x, \omega) \nabla U(x, \omega)) + C U(x, \omega) = F, \quad \forall x \in [0, 1], \quad (31)$$

with  $C = 15$ ,  $F = 10$  and following boundary conditions(BC):

$$U = 0 \text{ on } x = 0, \quad (32)$$

$$\hat{n} \cdot \nabla U = 1 \text{ on } x = 1. \quad (33)$$

Dirichlet BC on the left end and Neumann BC on the right end. The stochasticity in Eq. (31) arises from the uncertainty in the spatially-varying conductivity field  $A(x, \omega)$ . The logarithm of the conductivity  $A$  is modeled as a Gaussian random field:

$$\log A(x, \omega) \sim \text{GP}(\mu(x), k(x, x')), \quad (34)$$

where,  $\mu(x)$  and  $k(x, x')$  are the mean and covariance functions, respectively, of the Gaussian process. The mean function models beliefs about the generic trends of the conductivity field as a function of spatial location. For the sake of simplicity, we set  $\mu(x) = 0$  in this example. The covariance function  $k$  models beliefs about the regularity of the conductivity field and the lengthscales in which it varies. A popular choice for  $k$  is the exponential kernel:

$$k(x, x') = \sigma^2 \exp \left( -\frac{|x - x'|}{\ell} \right), \quad (35)$$

where  $\ell$  and  $\sigma$  represent the correlation length and standard deviation of the log conductivity field, respectively. We set  $\ell = 0.15$  and  $\sigma = 1$ . Strictly speaking, this  $A$  is not uniformly bounded below a.s., see stochastic ellipticity condition. However, this does not lead to any problems since in practice all the samples taken during the training process are uniformly bounded below.

First, we perform a preliminary dimensionality reduction on the stochastic process  $A$  using a truncated Karhunen-Loéve expansion(KLE) [60]:

$$\log A(x, \omega) \approx \log a(x, \Xi(\omega)) := \sum_{i=1}^{d_\xi} \Xi_i(\omega) \sqrt{\lambda_i} \phi_i(x), \quad (36)$$

where  $\Xi = (\Xi_1, \dots, \Xi_{d_\xi})$  with  $\Xi_i$  iid standard normal,  $\{\phi_i, \lambda_i\}$  are the eigenpairs of the correlation function  $k$ . The number of terms that we retain from the full KLE to capture 95% of the energy of the conductivity field is  $d_\xi = 28$ .

Following Eq. (18), we account for the Dirichlet boundary conditions by writing:

$$u(x, \Xi(\omega)) = x N(x, \Xi(\omega)). \quad (37)$$

We approximate  $N(x, \Xi(\omega))$  as  $\widehat{N}(x, \Xi(\omega); \theta)$  with a deep ResNet shown in Fig. 1b which accepts  $m = d + d_\xi = 1 + 28 = 29$  inputs. The deep ResNet has a initial dense layer followed by 4 residual blocks each with 2 layers having 100 neurons each, i.e.,  $K = 4$ ,  $L = 2$ ,  $n = 100$  and a final dense layer. We perform 65,000 iterations of ADAM optimization on the objective function  $\hat{J}(\theta)$  from Eq. (28) with constant learning rate of  $10^{-3}$ , using  $N_\xi = 100$  replicas of normal random vector  $\Xi(\omega)$ ,  $N_x = 7$  uniformly distributed samples in  $\mathcal{X}$  and  $N_b = 4$  uniformly distributed samples on the Neumann boundary  $\Gamma_n$  in each iteration. Here  $|X| = 1$  and  $|X_b| = 1$ .

The solution predicted by our deep ResNet is verified against the solution given by the finite volume method (FVM) solver implemented in FiPy [72]. For this we discretize spatial domain  $[0, 1]$  into  $N_{\text{cells}} = 100$  cells. Samples from the random conductivity (from Eq. (34)) are evaluated at the cell centers and fed as input to the FiPy solver. Then, the solver estimates the corresponding numerical solution of the SBVP at these cell locations. We calculate the relative root mean square error ‘ $\mathcal{E}$ ’ as follows:

$$\mathcal{E} = \sqrt{\frac{\sum_{i=1}^{N_{\text{sam}}} \sum_{j=1}^{N_{\text{cells}}} (u_{i,j}^{\text{FVM}} - u_{i,j}^{\text{DNN}})^2}{\sum_{i=1}^{N_{\text{sam}}} \sum_{j=1}^{N_{\text{cells}}} (u_{i,j}^{\text{FVM}})^2}}, \quad (38)$$

where  $u_{i,j}^{\text{FVM}}$  is the FVM solution at the  $j^{\text{th}}$  cell center corresponding to the  $i^{\text{th}}$  sample of the conductivity field, and  $u_{i,j}^{\text{DNN}}$  is the predicted solution from our

deep ResNet corresponding to the same realization of the conductivity at the same cell center location. Using 1,000 conductivity samples, we estimate the error  $\mathcal{E}$  to be 3.11%.

We also evaluate the quality of the DNN predictions based on two metrics. One is relative  $L_2$  error metric which is defined as :

$$L_2(\mathbf{u}_{\text{DNN}}, \mathbf{u}_{\text{FVM}}) = \frac{\|\mathbf{u}_{\text{FVM}} - \mathbf{u}_{\text{DNN}}\|_2}{\|\mathbf{u}_{\text{FVM}}\|_2}, \quad (39)$$

where,  $\|\cdot\|_2$  is the standard Euclidean norm.  $\mathbf{u}_{\text{FVM}}$  and  $\mathbf{u}_{\text{DNN}}$  are the FVM solution vector and the DNN prediction vector corresponding to a particular realization of the conductivity field. We also check the coefficient of determination, (also known as the  $R^2$  score), which is defined as:

$$R^2 = 1 - \frac{\sum_{k=1}^{N_{\text{cells}}} (u_{\text{FVM},k} - u_{\text{DNN},k})^2}{\sum_{k=1}^{N_{\text{cells}}} (u_{\text{FVM},k} - \bar{u}_{\text{FVM}})^2}, \quad (40)$$

where,  $k$  indexes all the FVM cell centers,  $u_{\text{FVM},k}$  and  $u_{\text{DNN},k}$  are the FVM solution and DNN predicted solution at the  $k^{\text{th}}$  cell center respectively, and  $\bar{u}_{\text{FVM}}$  is the mean of  $u_{\text{FVM},k}$ .

In Fig. 2, we compare the DNN solution with the FVM solution for few randomly selected sample cases. We observe that the DNN solution slightly misses FVM solution at the Neumann boundary end for few samples. We also observe that the relative  $L_2$  error as reported on the headers of the solution response is less than 0.06 and the  $R^2$  score close to 0.99, which implies that the predicted solution from the DNN matches the ground truth FVM solution very closely. Fig. 3 shows the histograms of the relative  $L_2$  error and  $R^2$  score for the 1000 samples.

Now using our trained ResNet we solve an uncertainty propagation problem. We draw  $10^5$  MC samples of conductivity and propagate them through the network to estimate the mean, variance and the PDF at  $x = 0.505$ . We compare these estimates to those obtained using the FVM solver. Fig. 4 shows the comparison plots of output statistics from DNN and FVM solver and Tab. 1 shows the corresponding relative  $L_2$  error and  $R^2$  scores of the mean and variance.

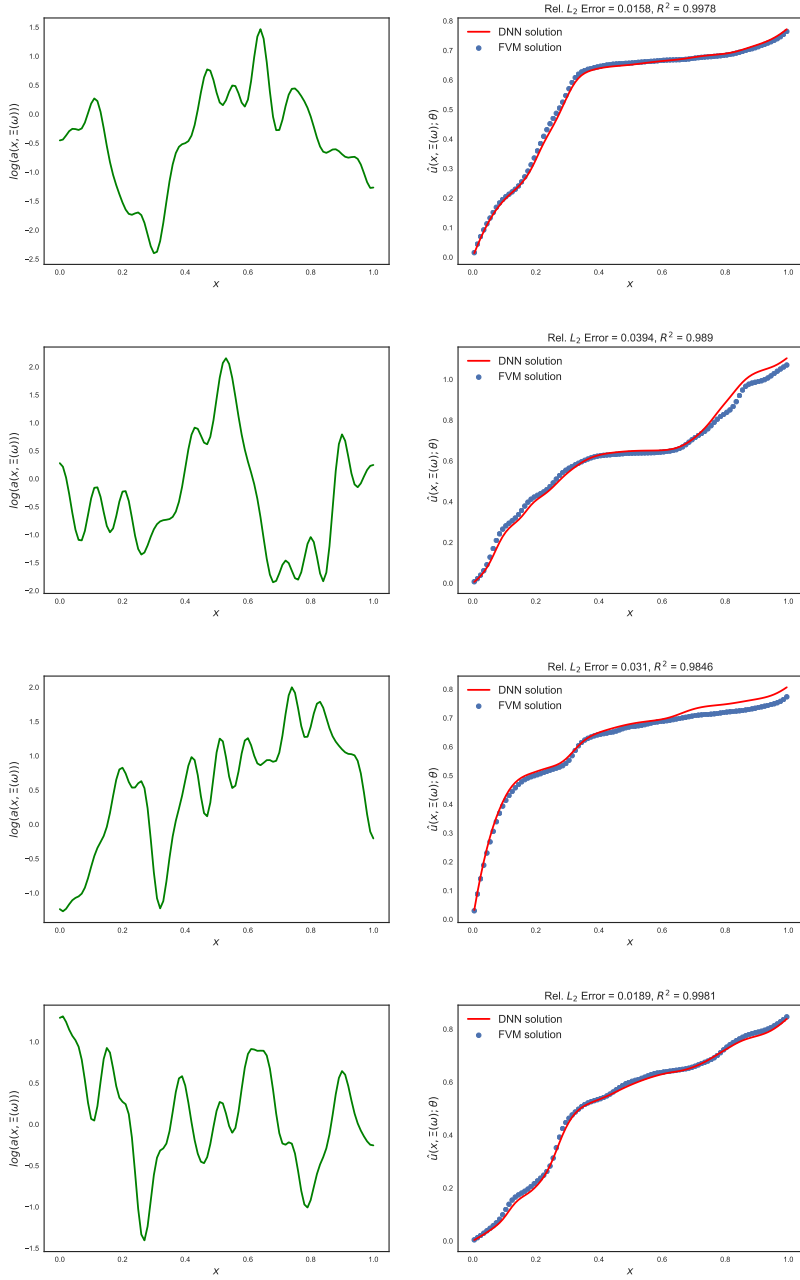
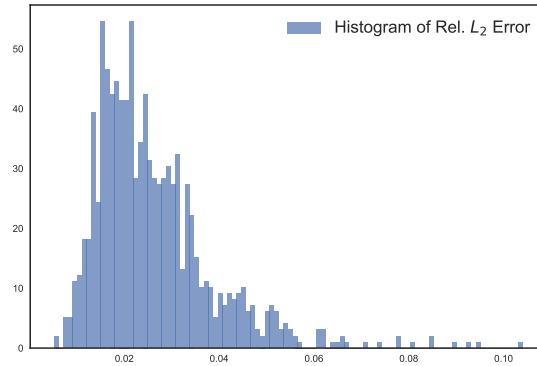


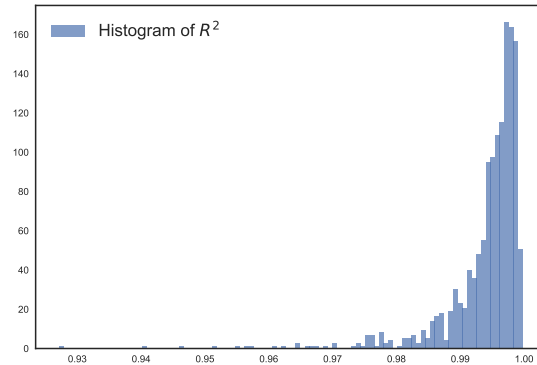
Figure 2: Example 1 (1D SBVP): Each row correspond to a sample case of random conductivity (left column) and the corresponding solution response (right column). The DNN solution is the red solid line and the FVM solution is the blue dotted line.

	Relative $L_2$ error	$R^2$ score
Mean	0.008	0.999
Variance	0.045	0.996

Table 1: Example 1 (1D SBVP): Relative  $L_2$  error and  $R^2$  scores of the mean and variance of the DNN SBVP. The true statistics are approximated using  $10^5$  MC samples of the FVM solver.

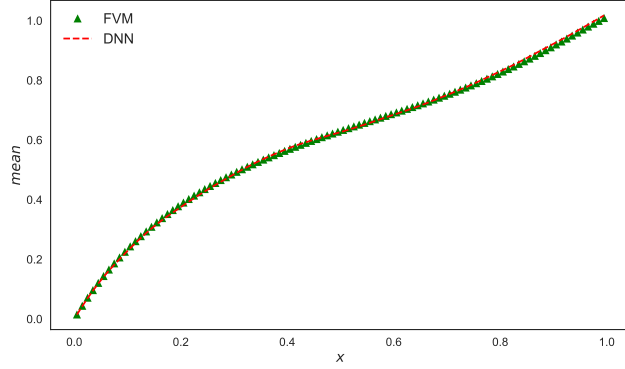


(a)

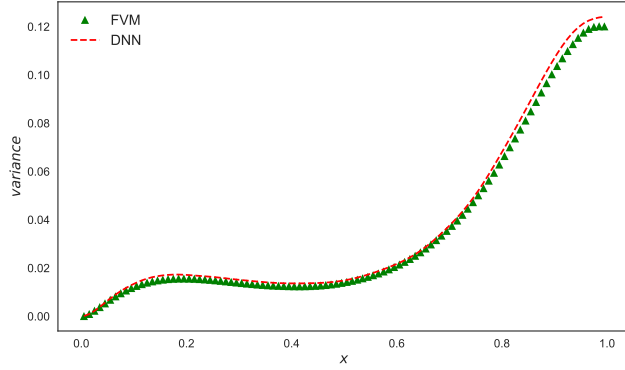


(b)

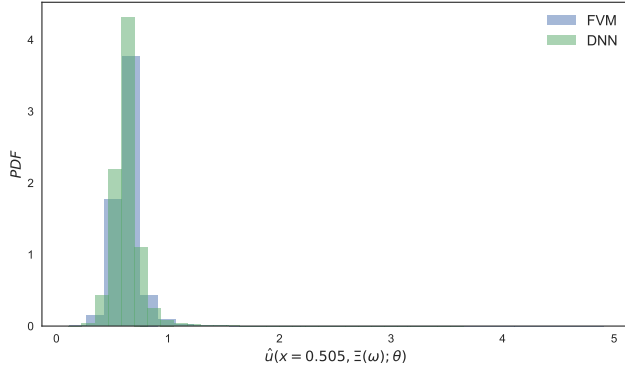
Figure 3: Example 1 (1D SBVP): 3a , 3b and shows the histogram of relative  $L_2$  error and  $R^2$  score for 1000 samples respectively.



(a)



(b)



(c)

Figure 4: Example 1 (1D SBVP): 4a, 4b and 4c shows the comparison plots of mean, variance and PDF respectively of SBVP solution from DNN and FVM solver for  $10^5$  MC samples.

Training DNN took 3.4 hours of computational time but once trained uncertainty propagation was done in 15 minutes with DNN solver for  $10^5$  samples.

### 3.2. Stochastic boundary value problem in 1D

Consider the following elliptic SBVP which models the steady-state heat conduction on a unit length domain:

$$-\nabla \cdot (A(x, \omega) \nabla U(x, \omega)) + C U(x, \omega) = F, \quad \forall x \in [0, 1], \quad (41)$$

with  $C = 15$ ,  $F = 10$  and subjected to Dirichlet boundary conditions on both ends

$$U = 1 \text{ on } x = 0, \quad (42)$$

$$U = 0 \text{ on } x = 1. \quad (43)$$

Similar to the previous example, we model the spatially-varying conductivity coefficient  $A(x, \omega)$  using a lognormal random field, i.e.,

$$\log A(x, \omega) \sim \text{GP}(\mu(x), k(x, x')), \quad (44)$$

with mean  $\mu(x) = 0$  and a exponential covariance

$$k(x, x') = \sigma^2 \exp \left( -\frac{|x - x'|}{\ell} \right), \quad (45)$$

We select the length scale and the variance of the field to be  $\ell = 0.03$  and  $\sigma = 1$ . We perform a preliminary dimensionality reduction on the stochastic process  $A(x, \omega)$  using a truncated KLE [60] and we retain  $d_\xi = 129$  terms corresponding to 95% energy of the conductivity field.

Following Eq. (18), we account for the Dirichlet boundary conditions by writing:

$$u(x, \Xi(\omega)) = (1 - x) + (x(1 - x))N(x, \Xi(\omega)). \quad (46)$$

We approximate  $N(x, \Xi(\omega))$  as  $\widehat{N}(x, \Xi(\omega); \theta)$  with a deep ResNet shown in Fig. 1b which accepts  $m = d + d_\xi = 1 + 129 = 130$  inputs. The deep ResNet has a initial dense layer followed by 3 residual blocks each with 2 layers having 400

	Relative $L_2$ error	$R^2$ score
Mean	0.010	0.999
Variance	0.079	0.982

Table 2: Example 2 (1D SBVP): Relative  $L_2$  error and  $R^2$  scores of the mean and variance of the DNN SBVP. The true statistics are approximated using  $10^5$  MC samples of the FVM solver.

neurons each, i.e.,  $K = 3$ ,  $L = 2$ ,  $n = 400$  and a final dense layer. We perform 65,000 iterations of ADAM optimization on the objective function  $\hat{J}(\theta)$  from Eq. (28) with constant learning rate of  $10^{-4}$ , using  $N_\xi = 100$  replicas of normal random vector  $\Xi(\omega)$  and  $N_x = 10$  uniformly distributed samples in  $\mathcal{X}$  in each iteration. Here  $|X| = 1$  and  $|X_b| = 1$ .

The solution predicted by our deep ResNet is again verified against the solution given by the FVM solver. For this we discretize the unit domain into  $N_{\text{cells}} = 100$  cells. Samples from the random conductivity (from Eq. (44)) are evaluated at the cell centers and fed as input to the FiPy solver. Then, the solver estimates the corresponding numerical solution of the SBVP at these cell locations. Using 1,000 conductivity samples, we estimate the error  $\mathcal{E}$ , see Eq. (38), to be 2.53%. In Fig. 5, we compare the DNN solution with the FVM solution for few randomly selected sample cases and we observe that the relative  $L_2$  error as reported on the headers of the predicted fields is less than 0.05 and the  $R^2$  score close to 0.997, which implies the predicted solution from DNN matches truth from FVM very closely. Fig. 6, shows the histograms of the relative  $L_2$  error and  $R^2$  score for the 1000 samples.

Now using our trained ResNet we solve an uncertainty propagation problem. We draw  $10^5$  MC samples of conductivity and propagate them through the network to estimate the mean, variance and the PDF at  $x = 0.505$ . We compare these estimates to those obtained using the FVM solver. Fig. 7 shows the comparison plots of output statistics from DNN and FVM solver and Tab. 2 shows the corresponding relative  $L_2$  error and  $R^2$  scores of the mean and variance.

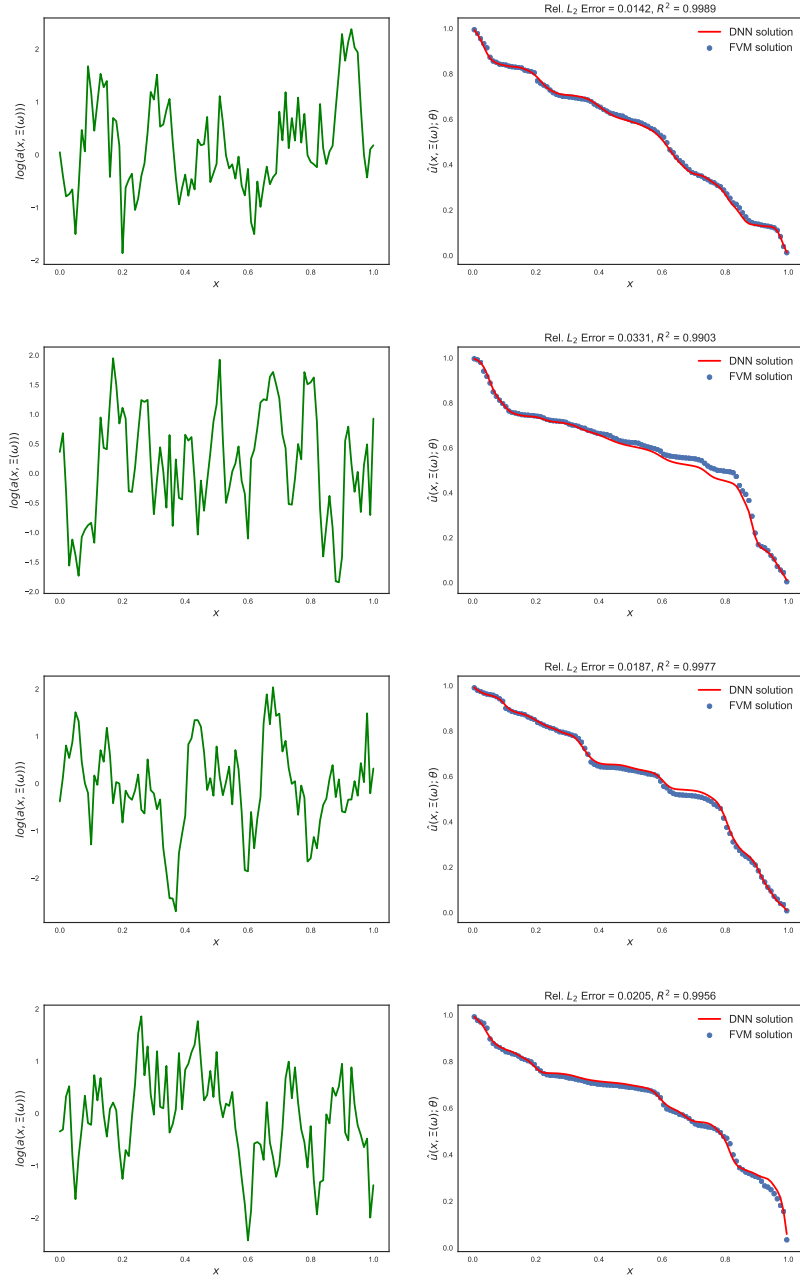
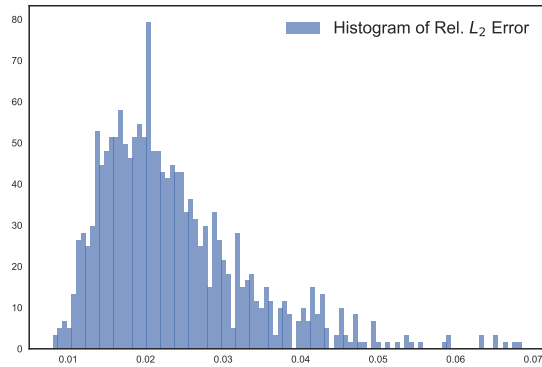
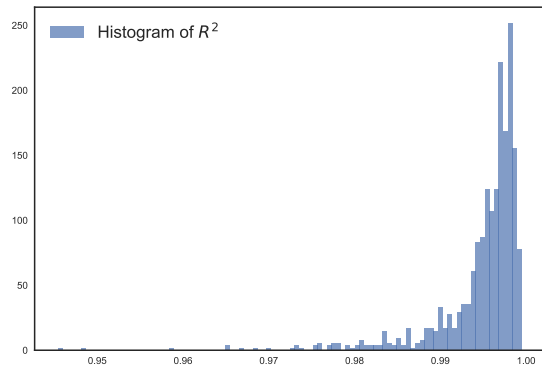


Figure 5: Example 2 (1D SBVP): Each row correspond to a sample case of random conductivity (left column) and the corresponding solution response (right column). The DNN solution is the red solid line and the FVM solution is the blue dotted line.

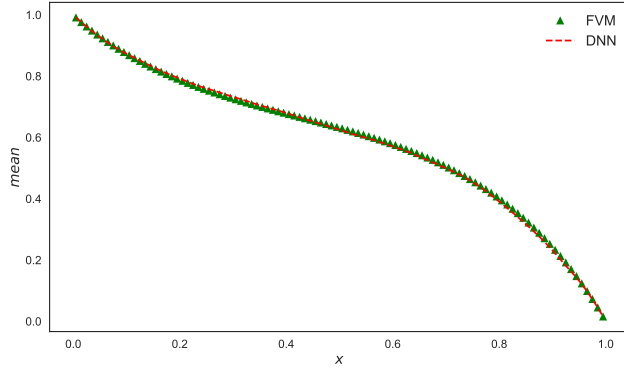


(a)

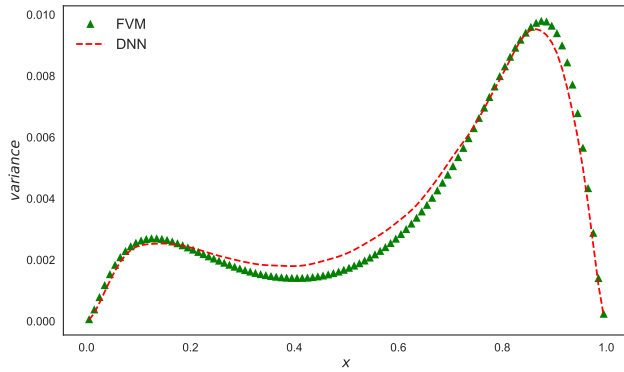


(b)

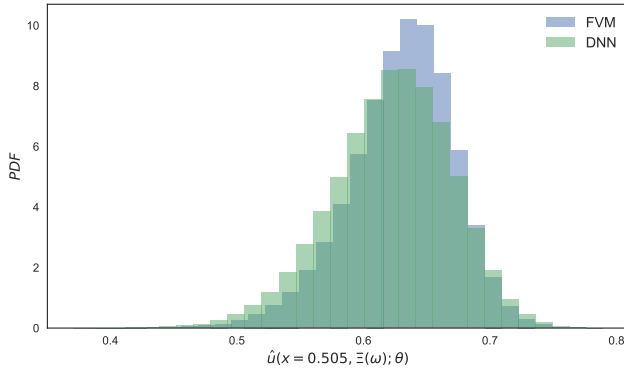
Figure 6: Example 2 (1D SBVP): 6a , 6b and shows the histogram of relative  $L_2$  error and  $R^2$  score for 1000 samples respectively.



(a)



(b)



(c)

Figure 7: Example 2 (1D SBVP): 7a, 7b and 7c shows the comparison plots of mean, variance and PDF respectively of SBVP solution from DNN and FVM solver for  $10^5$  MC samples.

Training DNN took 10 hours of computational time but once trained uncertainty propagation was done in 15 minutes with DNN solver for  $10^5$  samples.

### 3.3. Stochastic boundary value problem in 2D

Consider the following elliptic SBVP which models steady state heat conduction on the 2D unit square domain  $[0, 1]^2$ :

$$-\nabla \cdot (A(x, \omega) \nabla U(x, \omega)) + C U(x, \omega) = F, \quad \forall x \in [0, 1]^2, \quad (47)$$

with  $C = 15$ ,  $F = 10$  and boundary conditions

$$U = 1, \quad \text{if } x_1 = 0, \quad (48)$$

$$U = 0, \quad \text{if } x_1 = 1, \quad (49)$$

$$n^T(x) \nabla U(x, \omega) = 0, \quad \text{if } x_2 = 0 \text{ or } x_2 = 1. \quad (50)$$

Note that in Eq. (47) coefficient  $A(x, \omega)$  is a  $2 \times 2$  diagonal matrix with diagonal elements as conductivity value i.e.,  $A_{ij}(x, \omega) = 0$  when  $i \neq j$  and  $A_{ii}(x, \omega) = A_{jj}(x, \omega) = \tilde{A}(x, \omega)$ . Similar to the previous example, we model the spatially-varying conductivity value  $\tilde{A}(x, \omega)$  using a lognormal random field, i.e.,

$$\log \tilde{A}(x, \omega) \sim \text{GP}(\mu(x), k(x, x')), \quad (51)$$

with mean  $\mu(x) = 0$  and a radial basis function (RBF) covariance:

$$k(x, x') = \sigma^2 \exp \left( -\sum_{i=1}^2 \frac{\|x_i - x'_i\|^2}{2\ell_i^2} \right), \quad (52)$$

We select the length scales and the variance of the field to be  $\ell_1 = 0.05$ ,  $\ell_2 = 0.08$  and  $\sigma = 1.0$ . We perform a preliminary dimensionality reduction on the stochastic process  $\tilde{A}(x, \omega)$  using a truncated KLE and we retain  $d_\xi = 218$  terms corresponding to 99% energy of the conductivity field.

Following Eq. (18), we account for the Dirichlet boundary conditions as follows:

$$u(x, \Xi(\omega)) = (1 - x_1) + (x_1(1 - x_1))N(x, \Xi(\omega)). \quad (53)$$

As before, we approximate  $N(x, \Xi(\omega))$  as  $\widehat{N}(x, \Xi(\omega); \theta)$  with a deep ResNet shown in Fig. 1b that accepts  $m = d + d_\xi = 2 + 218 = 220$  input neurons. The

deep ResNet has a initial dense layer followed by 5 residual blocks each with 2 layers having 300 neurons each, i.e.,  $K = 5$ ,  $L = 2$ ,  $n = 300$  and a final dense layer. We perform 100,000 iterations of ADAM optimization on the objective function  $\hat{J}(\theta)$  from Eq. (28) with constant learning rate of  $10^{-4}$ , using  $N_\xi = 50$  replicas of normal random vector  $\Xi(\omega)$ ,  $N_x = 9$  uniformly distributed samples in  $\mathcal{X}$  and  $N_{b1}, N_{b2} = (3, 3)$  on each of the Neumann boundary in each iteration. Here  $|X| = 1$  and  $|X_b| = 1$ .

The solution predicted by our deep ResNet is again verified against the solution given by the FVM solver. For this we discretize the unit square domain into  $N_{\text{cells}} = 32 \times 32 = 1,024$  cells. Samples from the random conductivity (from Eq. (51)) are evaluated at the cell centers and fed as input to the FiPy solver. Then, the solver estimates the corresponding numerical solution of the SBVP at these cell locations. Using 1,000 conductivity samples, we estimate the error  $\mathcal{E}$ , see Eq. (38), to be 3.26%. In Fig. 8, we compare the DNN solution with the FVM solution for few randomly selected sample cases and we observe that the relative  $L_2$  error as reported on the headers of the predicted fields is less than 0.05 and the  $R^2$  score close to 0.995, which implies the predicted solution from DNN matches truth from FVM very closely. Fig. 9, shows the histograms of the relative  $L_2$  error and  $R^2$  score for the 1000 samples.

Now using our trained ResNet we solve an uncertainty propagation problem. We draw  $10^5$  MC samples of conductivity and propagate them through the network to estimate the mean, variance and the PDF of  $x = (0.515, 0.515)$  and  $x = (0.359, 0.734)$ . We compare these estimates to those obtained using the FVM solver. Figs. 10, 11 and 12 shows the comparison plots of output statistics from DNN and FVM solver and Tab. 3 shows the corresponding relative  $L_2$  error and  $R^2$  scores of the mean and variance.

Training DNN took 31.5 hours of computational time but once trained uncertainty propagation was done in 25 minutes with DNN solver for  $10^5$  samples.

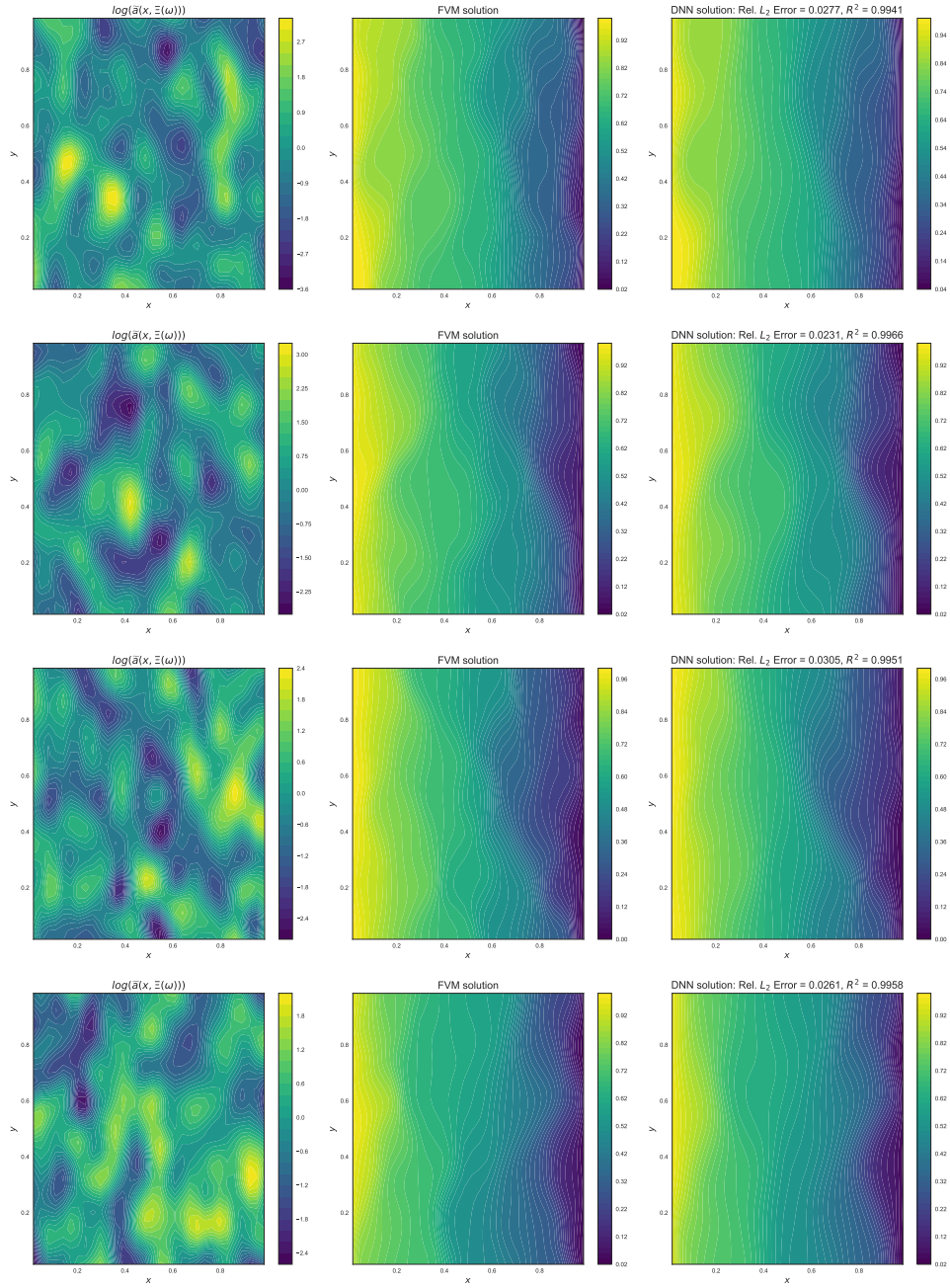
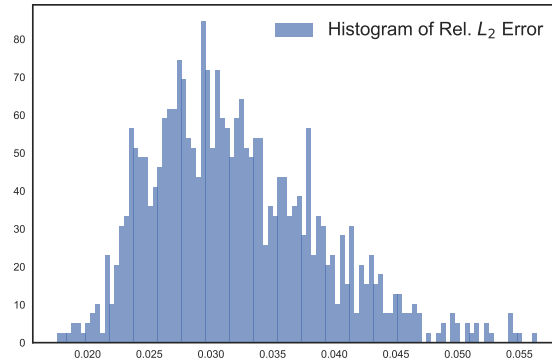


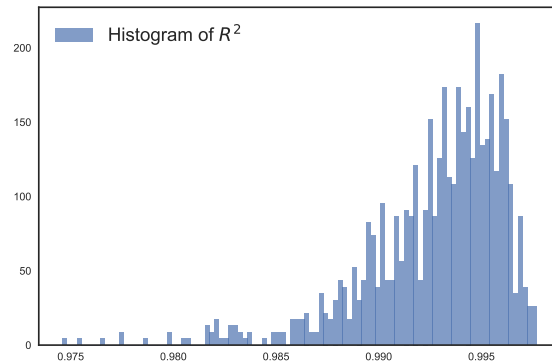
Figure 8: Example 3 (2D SBVP): Each row corresponds to a realization of the logarithm of the conductivity field,  $\log(\tilde{a}(x, \Xi(\omega)))$  (left column) and the corresponding solution response from FVM and DNN (middle and right columns)

	Relative $L_2$ error	$R^2$ score
Mean	0.0125	0.998
Variance	0.1036	0.966

Table 3: Example 3 (2D SBVP): Relative  $L_2$  error and  $R^2$  scores of the mean and variance of the DNN SBVP. The true statistics are approximated using  $10^5$  MC samples of the FVM solver.



(a)



(b)

Figure 9: Example 3 (2D SBVP): 9a , 9b and shows the histogram of relative  $L_2$  error and  $R^2$  score for 1000 samples respectively.

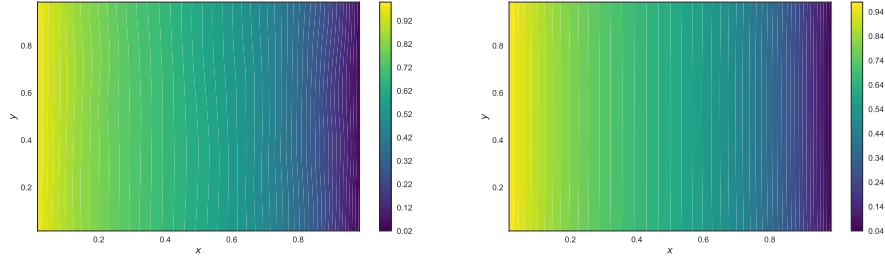


Figure 10: Example 3 (2D SBVP): Comparison of the mean of the SBVP solution from DNN (left figure) and FVM solver (right figure) for  $10^5$  MC samples

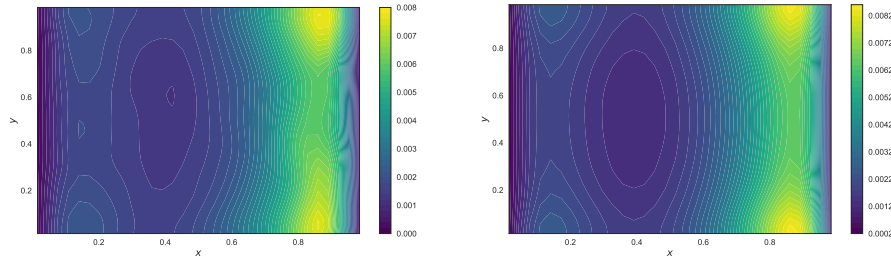


Figure 11: Example 3 (2D SBVP): Comparison of the variance of the SBVP solution from DNN (left figure) and FVM solver (right figure) for  $10^5$  MC samples

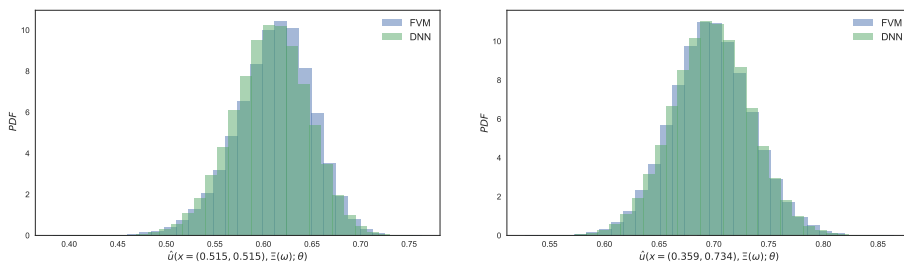


Figure 12: Example 3 (2D SBVP): Comparison of the PDF at two locations (at  $x = (0.515, 0.515)$  (left figure) and  $x = (0.359, 0.734)$  (right figure)) from DNN and FVM solver for  $10^5$  MC samples

## 4. Conclusion

We developed a methodology for solving SBVPs with high-dimensional uncertainties. The characteristic of our technique is that it does not require an external solver as it makes direct use of the physics of the problem. We recasted the SBVP in a variational form and we showed that it has a unique solution in a suitable function space. Then, we minimized the corresponding energy functional within the space of DNNs that automatically satisfy the Dirichlet conditions. Within this functional subspace, we derived a stochastic optimization problem with the same solution by deriving an unbiased estimator of the energy functional. We solved this stochastic optimization problem using a standard variant of stochastic gradient descent.

We solved three SBVPs, two in one dimension and one in two spatial dimensions with 28, 129 and 218 stochastic dimensions respectively, and we compared our results to a standard FVM solver endowed with MC sampling. The relative root mean square error for each SBVP was 3.11%, 2.53% and 3.26%, respectively for 1000 samples. In uncertainty propagation tasks, the method estimated the mean with smaller than 1.3% relative  $L_2$  error and the variance with less than 10.5% relative  $L_2$  error.

Despite the promising results, the current approach requires further development to become competitive with the current state of the art. First, even though it scales well to higher dimensions, it is computationally demanding and, thus, it could benefit from parallelization. Second, there is a need for techniques that can automatically enforce the Dirichlet boundary condition without the need for manual construction of a trial solution to enforce them, see for example the promising approach of [73]. Third, the unbiased estimator we constructed to make the methodology amenable to stochastic gradient decent was the simplest possible choice. In the future work we will develop other estimators with smaller variance and, thus, accelerate the convergence of stochastic optimization. Finally, and most importantly, the behavior of the energy functional loss in the space of neural networks should be understood and studied further analytically.

## Acknowledgements

We would like to acknowledge support from the NSF awards #1737591 and #1728165. We would also like to acknowledge support from the Defense Advanced Research Projects Agency (DARPA) under the Physics of Artificial Intelligence (PAI) program (contract HR00111890034).

## References

### References

- [1] D. A. Reed, J. Dongarra, Exascale computing and big data, *Communications of the ACM* 58 (2015) 56–68.
- [2] H. P. Langtangen, Computational partial differential equations: numerical methods and diffpack programming, volume 2, Springer Berlin, 1999.
- [3] R. C. Smith, Uncertainty quantification: theory, implementation, and applications, volume 12, Siam, 2013.
- [4] T. J. Sullivan, Introduction to uncertainty quantification, volume 63, Springer, 2015.
- [5] C. Robert, G. Casella, Monte Carlo statistical methods, Springer Science & Business Media, 2013.
- [6] I. G. Graham, M. J. Parkinson, R. Scheichl, Modern monte carlo variants for uncertainty quantification in neutron transport, in: *Contemporary Computational Mathematics-A Celebration of the 80th Birthday of Ian Sloan*, Springer, 2018, pp. 455–81.
- [7] K. A. Cliffe, M. B. Giles, R. Scheichl, A. L. Teckentrup, Multilevel monte carlo methods and applications to elliptic pdes with random coefficients, *Computing and Visualization in Science* 14 (2011) 3.

- [8] F. Y. Kuo, C. Schwab, I. H. Sloan, Quasi-monte carlo finite element methods for a class of elliptic partial differential equations with random coefficients, *SIAM Journal on Numerical Analysis* 50 (2012) 3351–74.
- [9] J. Dick, R. N. Gantner, Q. T. L. Gia, C. Schwab, Higher order quasi-monte carlo integration for bayesian estimation, *arXiv preprint arXiv:1602.07363* (2016).
- [10] M. Sambridge, K. Mosegaard, Monte carlo methods in geophysical inverse problems, *Reviews of Geophysics* 40 (2002) 3–1.
- [11] S. Sankararaman, Y. Ling, S. Mahadevan, Uncertainty quantification and model validation of fatigue crack growth prediction, *Engineering Fracture Mechanics* 78 (2011) 1487–504.
- [12] S. Isukapalli, A. Roy, P. Georgopoulos, Stochastic response surface methods (srsms) for uncertainty propagation: application to environmental and biological systems, *Risk analysis* 18 (1998) 351–63.
- [13] P. Angelikopoulos, C. Papadimitriou, P. Koumoutsakos, Bayesian uncertainty quantification and propagation in molecular dynamics simulations: a high performance computing framework, *The Journal of chemical physics* 137 (2012) 144103.
- [14] B. A. Lockwood, M. Anitescu, Gradient-enhanced universal kriging for uncertainty propagation, *Nuclear Science and Engineering* 170 (2012) 168–95.
- [15] J. D. Martin, T. W. Simpson, Use of kriging models to approximate deterministic computer models, *AIAA journal* 43 (2005) 853–63.
- [16] I. Bilionis, N. Zabaras, Multi-output local gaussian process regression: Applications to uncertainty quantification, *Journal of Computational Physics* 231 (2012) 5718–46.

- [17] I. Bilionis, N. Zabaras, B. A. Konomi, G. Lin, Multi-output separable gaussian process: Towards an efficient, fully bayesian paradigm for uncertainty quantification, *Journal of Computational Physics* 241 (2013) 212–39.
- [18] P. Chen, N. Zabaras, I. Bilionis, Uncertainty propagation using infinite mixture of gaussian processes and variational bayesian inference, *Journal of Computational Physics* 284 (2015) 291–333.
- [19] R. Tripathy, I. Bilionis, M. Gonzalez, Gaussian processes with built-in dimensionality reduction: Applications to high-dimensional uncertainty propagation, *Journal of Computational Physics* 321 (2016) 191–223.
- [20] H. N. Najm, Uncertainty quantification and polynomial chaos techniques in computational fluid dynamics, *Annual review of fluid mechanics* 41 (2009) 35–52.
- [21] M. Eldred, J. Burkardt, Comparison of non-intrusive polynomial chaos and stochastic collocation methods for uncertainty quantification, in: 47th AIAA aerospace sciences meeting including the new horizons forum and aerospace exposition, 2009, p. 976.
- [22] D. Xiu, G. E. Karniadakis, The wiener–askey polynomial chaos for stochastic differential equations, *SIAM journal on scientific computing* 24 (2002) 619–44.
- [23] O. G. Ernst, A. Mugler, H.-J. Starkloff, E. Ullmann, On the convergence of generalized polynomial chaos expansions, *ESAIM: Mathematical Modelling and Numerical Analysis* 46 (2012) 317–39.
- [24] R. G. Regis, C. A. Shoemaker, Combining radial basis function surrogates and dynamic coordinate search in high-dimensional expensive black-box optimization, *Engineering Optimization* 45 (2013) 529–55.
- [25] S. Volpi, M. Diez, N. J. Gaul, H. Song, U. Iemma, K. Choi, E. F. Campana, F. Stern, Development and validation of a dynamic metamodel based on

stochastic radial basis functions and uncertainty quantification, *Structural and Multidisciplinary Optimization* 51 (2015) 347–68.

- [26] E. Keogh, A. Mueen, Curse of dimensionality, in: *Encyclopedia of machine learning*, Springer, 2011, pp. 257–8.
- [27] P. Constantine, Active subspaces: Emerging ideas for dimension reduction in parameter studies, <https://speakerdeck.com/paulcon/active-subspaces-emerging-ideas-for-dimension-reduction-in-parameter-studies-1>, 2016.
- [28] A. Saltelli, K. Chan, E. M. Scott, et al., *Sensitivity analysis*, volume 1, Wiley New York, 2000.
- [29] R. M. Neal, Assessing relevance determination methods using delve, *Nato Asi Series F Computer And Systems Sciences* 168 (1998) 97–132.
- [30] R. Ghanem, Stochastic finite elements with multiple random non-gaussian properties, *Journal of Engineering Mechanics* 125 (1999) 26–40.
- [31] I. Jolliffe, Principal component analysis, in: *International encyclopedia of statistical science*, Springer, 2011, pp. 1094–6.
- [32] B. Schölkopf, A. Smola, K.-R. Müller, Kernel principal component analysis, in: *International Conference on Artificial Neural Networks*, Springer, 1997, pp. 583–8.
- [33] X. Ma, N. Zabaras, Kernel principal component analysis for stochastic input model generation, *Journal of Computational Physics* 230 (2011) 7311–31.
- [34] P. G. Constantine, E. Dow, Q. Wang, Active subspace methods in theory and practice: applications to kriging surfaces, *SIAM Journal on Scientific Computing* 36 (2014) A1500–24.
- [35] P. Constantine, D. Gleich, Computing active subspaces with monte carlo, arXiv preprint arXiv:1408.0545 (2014).

- [36] T. W. Lukaczyk, P. Constantine, F. Palacios, J. J. Alonso, Active subspaces for shape optimization, in: 10th AIAA Multidisciplinary Design Optimization Conference, 2014, p. 1171.
- [37] J. L. Jefferson, J. M. Gilbert, P. G. Constantine, R. M. Maxwell, Active subspaces for sensitivity analysis and dimension reduction of an integrated hydrologic model, *Computers & Geosciences* 83 (2015) 127–38.
- [38] P. G. Constantine, M. Emory, J. Larsson, G. Iaccarino, Exploiting active subspaces to quantify uncertainty in the numerical simulation of the hyshot ii scramjet, *Journal of Computational Physics* 302 (2015) 1–20.
- [39] P. G. Constantine, C. Kent, T. Bui-Thanh, Accelerating markov chain monte carlo with active subspaces, *SIAM Journal on Scientific Computing* 38 (2016) A2779–805.
- [40] M. Tezzele, F. Ballarin, G. Rozza, Combined parameter and model reduction of cardiovascular problems by means of active subspaces and pod-galerkin methods, in: Mathematical and Numerical Modeling of the Cardiovascular System and Applications, Springer, 2018, pp. 185–207.
- [41] R. Tripathy, I. Bilionis, Deep uq: Learning deep neural network surrogate models for high dimensional uncertainty quantification, *arXiv preprint arXiv:1802.00850* (2018).
- [42] Y. Zhu, N. Zabaras, Bayesian deep convolutional encoder–decoder networks for surrogate modeling and uncertainty quantification, *Journal of Computational Physics* 366 (2018) 415–47.
- [43] S. Mo, Y. Zhu, J. Zabaras, Nicholas, X. Shi, J. Wu, Deep convolutional encoder-decoder networks for uncertainty quantification of dynamic multiphase flow in heterogeneous media, *Water Resources Research* (2018).
- [44] K. He, X. Zhang, S. Ren, J. Sun, Deep residual learning for image recognition, in: Proceedings of the IEEE conference on computer vision and pattern recognition, 2016, pp. 770–8.

- [45] A. G. Baydin, B. A. Pearlmutter, A. A. Radul, Automatic differentiation in machine learning: a survey, *CoRR* abs/1502.05767 (2015).
- [46] T. Qin, K. Wu, D. Xiu, Data driven governing equations approximation using deep neural networks, *arXiv preprint arXiv:1811.05537* (2018).
- [47] I. Goodfellow, Y. Bengio, A. Courville, Y. Bengio, *Deep learning*, volume 1, MIT press Cambridge, 2016.
- [48] K. Hornik, M. Stinchcombe, H. White, Multilayer feedforward networks are universal approximators, *Neural networks* 2 (1989) 359–66.
- [49] M. Abadi, P. Barham, J. Chen, Z. Chen, A. Davis, J. Dean, M. Devin, S. Ghemawat, G. Irving, M. Isard, et al., Tensorflow: a system for large-scale machine learning., in: *OSDI*, volume 16, 2016, pp. 265–83.
- [50] A. Paszke, S. Gross, S. Chintala, G. Chanan, E. Yang, Z. DeVito, Z. Lin, A. Desmaison, L. Antiga, A. Lerer, Automatic differentiation in pytorch (2017).
- [51] T. Chen, M. Li, Y. Li, M. Lin, N. Wang, M. Wang, T. Xiao, B. Xu, C. Zhang, Z. Zhang, Mxnet: A flexible and efficient machine learning library for heterogeneous distributed systems, *arXiv preprint arXiv:1512.01274* (2015).
- [52] D. P. Kingma, J. Ba, Adam: A method for stochastic optimization, *arXiv preprint arXiv:1412.6980* (2014).
- [53] T. Tieleman, G. Hinton, Lecture 6.5-rmsprop: Divide the gradient by a running average of its recent magnitude, *COURSERA: Neural networks for machine learning* 4 (2012) 26–31.
- [54] M. D. Zeiler, Adadelta: an adaptive learning rate method, *arXiv preprint arXiv:1212.5701* (2012).

- [55] M. Raissi, P. Perdikaris, G. E. Karniadakis, Physics informed deep learning (part i): Data-driven solutions of nonlinear partial differential equations, arXiv preprint arXiv:1711.10561 (2017).
- [56] M. Raissi, P. Perdikaris, G. E. Karniadakis, Physics informed deep learning (part ii): data-driven discovery of nonlinear partial differential equations, arXiv preprint arXiv:1711.10566 (2017).
- [57] E. Weinan, B. Yu, The deep ritz method: A deep learning-based numerical algorithm for solving variational problems, *Communications in Mathematics and Statistics* 6 (2018) 1–12.
- [58] Y. Zhu, N. Zabaras, P.-S. Koutsourelakis, P. Perdikaris, Physics-constrained deep learning for high-dimensional surrogate modeling and uncertainty quantification without labeled data, arXiv preprint arXiv:1901.06314 (2019).
- [59] R. A. Adams, J. J. Fournier, *Sobolev spaces*, volume 140, Elsevier, 2003.
- [60] W. Betz, I. Papaioannou, D. Straub, Numerical methods for the discretization of random fields by means of the karhunen–loève expansion, *Computer Methods in Applied Mechanics and Engineering* 271 (2014) 109–29.
- [61] D. Ting, M. I. Jordan, On nonlinear dimensionality reduction, linear smoothing and autoencoding, arXiv preprint arXiv:1803.02432 (2018).
- [62] R. Fletcher, *Practical methods of optimization*, John Wiley & Sons, 2013.
- [63] I. E. Lagaris, A. Likas, D. I. Fotiadis, Artificial Neural Networks for Solving Ordinary and Partial Differential Equations, *ArXiv Physics e-prints* (1997).
- [64] J. Berg, K. Nyström, A unified deep artificial neural network approach to partial differential equations in complex geometries, *ArXiv e-prints* (2017).
- [65] C. Szegedy, S. Ioffe, V. Vanhoucke, A. A. Alemi, Inception-v4, inception-resnet and the impact of residual connections on learning., in: *AAAI*, volume 4, 2017, p. 12.

- [66] Z. Wu, C. Shen, A. Van Den Hengel, Wider or deeper: Revisiting the resnet model for visual recognition, *Pattern Recognition* (2019).
- [67] A. Veit, M. J. Wilber, S. Belongie, Residual networks behave like ensembles of relatively shallow networks, in: *Advances in Neural Information Processing Systems*, 2016, pp. 550–8.
- [68] P. Ramachandran, B. Zoph, Q. V. Le, Swish: a self-gated activation function, *arXiv preprint arXiv:1710.05941* (2017).
- [69] L. Bottou, Large-scale machine learning with stochastic gradient descent, in: *Proceedings of COMPSTAT'2010*, Springer, 2010, pp. 177–86.
- [70] M. Abadi, A. Agarwal, P. Barham, E. Brevdo, Z. Chen, C. Citro, G. S. Corrado, A. Davis, J. Dean, M. Devin, S. Ghemawat, I. J. Goodfellow, A. Harp, G. Irving, M. Isard, Y. Jia, R. Józefowicz, L. Kaiser, M. Kudlur, J. Levenberg, D. Mané, R. Monga, S. Moore, D. G. Murray, C. Olah, M. Schuster, J. Shlens, B. Steiner, I. Sutskever, K. Talwar, P. A. Tucker, V. Vanhoucke, V. Vasudevan, F. B. Viégas, O. Vinyals, P. Warden, M. Wattenberg, M. Wicke, Y. Yu, X. Zheng, Tensorflow: Large-scale machine learning on heterogeneous distributed systems, *CoRR* abs/1603.04467 (2016).
- [71] Y. Chauvin, D. E. Rumelhart, *Backpropagation: theory, architectures, and applications*, Psychology Press, 1995.
- [72] J. E. Guyer, D. Wheeler, J. A. Warren, Fipy: partial differential equations with python, *Computing in Science & Engineering* 11 (2009).
- [73] J. Berg, K. Nyström, A unified deep artificial neural network approach to partial differential equations in complex geometries, *Neurocomputing* 317 (2018) 28–41.